Determination of deformation potentials in ZnSe/GaAs strained-layer heterostructures

F. Kubacki and J. Gutowski
Institut für Festkörperphysik, Universität Bremen, D-28334 Bremen, Germany

D. Hommel
Institut für Festkörperphysik, Universität Bremen, D-28334 Bremen, Germany
and Physikalisches Institut, Universität Würzburg, D-97074 Würzburg, Germany

M. Heuken
Institut für Halbleitertechnik, Rheinisch-Westfälische Technische Hochschule Aachen, D-52026 Aachen, Germany

U. W. Pohl
Institut für Festkörperphysik, Technische Universität Berlin, D-10623 Berlin, Germany
(Received 21 December 1995)

A method to determine the deformation potentials in strained-layer heterostructures is introduced. This is done by measuring the piezoreflectance of biaxially strained ZnSe/GaAs layers under additional application of an external uniaxial stress along the (110) axis. The resulting lowered crystal symmetry yields four dipole-allowed eigenstates for the $1S$ exciton. By using a model that includes strain as well as excitonic spatial dispersion and exchange effects we are able to determine the internal biaxial strain, the exchange splitting, and the deformation potentials. The numerical results obtained on ZnSe/GaAs heterostructures as a model system are compared with the deformation potentials given by measurements at bulk ZnSe crystals. [S0163-1829(96)05527-0]

I. INTRODUCTION

In recent years there has been a rising interest in the fabrication of blue-emitting laser diodes.[1,2] These devices, based on ZnSe composite materials containing Cd, S, and Mg at different concentrations, consist of heterostructures often involving multiple quantum wells. Because of the different lattice constants of the subsequently overgrown materials the structures are usually lattice mismatched; i.e., one obtains a built-in biaxial strain in the layers. To describe the effect of strain on the electronic band structure knowledge of the deformation potentials of the different materials is required. This paper presents a method to determine these relevant parameters.

The system under consideration—high-quality ZnSe/GaAs epilayers—serves as a model system for a strained-layer heterostructure. In the case of epitaxial growth of II-VI semiconductors the difficulties to obtain II-VI substrates of sufficient structural perfection and dopability require heteroepitaxial growth. GaAs used as a substrate material for the most ZnSe-based device structures exhibits a lattice mismatch of 0.28% to ZnSe yielding a compressive strain in the ZnSe epilayer. Moreover, as the heteroepitaxial structure is cooled down to a certain measuring temperature (here, 1.6 K), the different thermal expansion coefficients cause a tensile-strain contribution. The built-in biaxial strain resulting from both effects lowers the crystal symmetry from T_d to D_{2d}, and hence modifies the electronic properties. This induces a light-hole (lh)–heavy-hole (hh) splitting of the valence band and leads to the appearance of the two respective free excitons.[3] Thus, measuring the exciton energies gives information about the strain situation in the surface region of the layer within the penetration depth of the exciting light. Due to the large exciton binding and exchange energies, ZnSe is an excellent model material to demonstrate the approach to determine deformation potentials, as will be described in the following.

Mayer *et al.*[4] and Permogorov *et al.*[5] studied the exciton polariton in biaxially strained ZnSe/GaAs heterostructures. They used resonant Brillouin scattering to get the internal strain and exchange parameters. For the determination of deformation potentials it is highly desirable to ensure that one has a well-known strain situation. This is done by additionally applying an external stress. Several authors studied the influence of hydrostatic pressure on the behavior of the exciton in ZnSe.[6–8] The application of an external uniaxial stress[9–11] advantageously reduces the symmetry of the crystal so that the degeneracy of the eight $1S$ exciton states is removed. Thus, we have investigated the effect of externally applied uniaxial stress on the excitonic reflectance of biaxially prestrained ZnSe/GaAs heterostructures. The uniaxial pressure is directed along the (110) axis while the ZnSe layers are grown in the (001) direction. Consequently, the overlap of external stress and growth-induced biaxial strain further lowers the crystal symmetry from D_{2d} to C_{2v}. By varying the polarization of the exciting light we could observe the stress-induced shift and splitting of four different exciton polaritons. A line-shape analysis yields the exact position of the exciton resonances. The pressure dependence of these resonances is calculated using a model analogous to the formalism introduced by Cho[12] in which we have to consider excitonic exchange and strain effects simultaneously. It is possible to determine the trigonal deformation potential in epilayers that are grown in the (001) direction. Futhermore,

the exchange parameter, the internal strain, and the hydrostatic deformation potential are obtained. In order to confirm the determined deformation potential values we have comparatively investigated ZnSe bulk material under uniaxial stress applied in the (111) direction.

II. EXPERIMENT

The epilayers used in this study were grown by molecular beam epitaxy (MBE) in the Physikalisches Institut in Würzburg and by metalorganic vapor phase epitaxy (MOVPE) in the Institut für Halbleitertechnik, RWTH Aachen. The growth temperatures were 300 °C and 480 °C for the MBE (Ref. 13) and the MOVPE (Ref. 14) layers, respectively. Thus, the samples exhibit tensile strain at their surfaces at the measuring temperature. The heterostructures are rectangular parallelepipeds with the long axis parallel to (110).

ZnSe bulk crystals were grown in a closed tube by seeded vapor phase transport in a hydrogen ambient at 1190 °C with a thermal gradient of 10 °C to the source material. Here, the externally stressed surfaces were just polished with 3-μm Al_2O_3 powder to obtain flat plains that yield a homogeneous stress situation in the sample.

The reflection spectra were recorded by using a 150-W tungsten halogen lamp as light source. With regard to the heterostructure the wave vector of the incident light is nearly parallel to the (001) growth direction while the electric field vector was adjusted parallel or perpendicular to the (110) external stress axis. For detection we used a 1-m Spex monochromator (resolution $\leqslant 0.07$ meV) and a bialkali photomultiplier. To apply stress along the (110) direction the epilayers were simply cleaved perpendicular to this axis. The cleaved edges are sufficiently plain and parallel to guarantee for an almost homogeneous pressure distribution caused by the uniaxial stress apparatus. For the setup of the pressure apparatus, which was constructed at the Universität Bremen, we used a sample mounting head similar to that of Balslev.[15] The epilayers were mounted between two steel pistons. The lower piston is pulled by a tie rod. The pressure tuning is done by using a spring balance. To perform measurements at 1.6 K, the apparatus has to work in a He immersion cryostat under vacuum conditions. For this purpose, the connection of the tie rod with the spring balance is covered by a vacuum-safe bellows construction.

III. THEORY

A. Group theory and selection rules

Considerations based on group theory and their application to the measured polarization dependence offer the possibility to recognize the symmetry of the observed resonances. In the unstrained zinc-blende material (point group T_d) the exciton is formed by a Γ_6 conduction band electron and a Γ_8 valence band hole. By taking into account a Γ_1 envelope function for the $1S$ state the eightfold exciton ground state can be decomposed into its irreducible components[16]

$$\Gamma_6 \otimes \Gamma_8 \otimes \Gamma_1 = \Gamma_3 \oplus \Gamma_4 \oplus \Gamma_5. \tag{1}$$

The respective exciton wave functions[12] consist of linear combinations of the electron and hole band functions $|m_e, m_j\rangle$ with $|m_e\rangle = |\pm\tfrac{1}{2}\rangle$ and $|m_j\rangle = |\pm\tfrac{1}{2}\rangle, |\pm\tfrac{3}{2}\rangle$:

$$\Gamma_3 : |2,+\rangle = \frac{1}{\sqrt{2}} \left(|\tfrac{1}{2},-\tfrac{1}{2}\rangle + |-\tfrac{1}{2},\tfrac{1}{2}\rangle \right),$$

$$\Gamma_3 : |2,0\rangle = -\frac{1}{\sqrt{2}} \left(|\tfrac{1}{2},\tfrac{3}{2}\rangle + |-\tfrac{1}{2},-\tfrac{3}{2}\rangle \right),$$

$$\Gamma_4 : |1,+\rangle = \frac{1}{2\sqrt{2}} \left(\sqrt{3}|\tfrac{1}{2},\tfrac{1}{2}\rangle + |-\tfrac{1}{2},\tfrac{3}{2}\rangle + |\tfrac{1}{2},-\tfrac{3}{2}\rangle + \sqrt{3}|-\tfrac{1}{2},-\tfrac{1}{2}\rangle \right),$$

$$\Gamma_4 : |1,-\rangle = i\,\frac{1}{2\sqrt{2}} \left(\sqrt{3}|\tfrac{1}{2},\tfrac{1}{2}\rangle + |-\tfrac{1}{2},\tfrac{3}{2}\rangle - |\tfrac{1}{2},-\tfrac{3}{2}\rangle - \sqrt{3}|-\tfrac{1}{2},-\tfrac{1}{2}\rangle \right), \tag{2}$$

$$\Gamma_4 : |2,-\rangle = -\frac{1}{\sqrt{2}} \left(|\tfrac{1}{2},\tfrac{3}{2}\rangle - |-\tfrac{1}{2},-\tfrac{3}{2}\rangle \right),$$

$$\Gamma_5 : |x\rangle = \frac{1}{2\sqrt{2}} \left(|\tfrac{1}{2},\tfrac{1}{2}\rangle - \sqrt{3}|-\tfrac{1}{2},\tfrac{3}{2}\rangle - \sqrt{3}|\tfrac{1}{2},-\tfrac{3}{2}\rangle + |-\tfrac{1}{2},-\tfrac{1}{2}\rangle \right),$$

$$\Gamma_5 : |y\rangle = -i\,\frac{1}{2\sqrt{2}} \left(|\tfrac{1}{2},\tfrac{1}{2}\rangle - \sqrt{3}|-\tfrac{1}{2},\tfrac{3}{2}\rangle + \sqrt{3}|\tfrac{1}{2},-\tfrac{3}{2}\rangle - |-\tfrac{1}{2},-\tfrac{1}{2}\rangle \right),$$

$$\Gamma_5 : |z\rangle = -\frac{1}{\sqrt{2}} \left(|\tfrac{1}{2},-\tfrac{1}{2}\rangle - |-\tfrac{1}{2},\tfrac{1}{2}\rangle \right).$$

Since the dipole operator possesses Γ_5 symmetry in T_d, only the so-called Γ_5 orthoexcitons are dipole allowed whereas the Γ_4 paraexcitons are dipole forbidden. The externally applied stress along the (110) crystal axis of a biaxially strained epilayer that has been grown in the (001) direction reduces the symmetry to the point group C_{2v}. Therefore, the splitting pattern of the $1S$ exciton states reads[16]

$$T_d \rightarrow C_{2v}$$

$$\Gamma_3 \rightarrow \Gamma_1(|2,0\rangle) \oplus \Gamma_3(|2,+\rangle),$$

$$\Gamma_4 \rightarrow \Gamma_2(|1,+\rangle, |1,-\rangle) \oplus \Gamma_3(|2,-\rangle) \oplus \Gamma_4(|1,+\rangle, |1,-\rangle),$$

$$\Gamma_5 \rightarrow \Gamma_1(|z\rangle) \oplus \Gamma_2(|x\rangle, |y\rangle) \oplus \Gamma_4(|x\rangle, |y\rangle).$$

The reduction of symmetry to C_{2v} induces mixed states of symmetries Γ_2 and Γ_4 for the $|x\rangle$ and $|y\rangle$ orthoexcitons. Since the $|1,+\rangle$ and $|1,-\rangle$ paraexcitons also transform like Γ_2 and Γ_4, they interact with the dipole-allowed orthoexcitons and consequently attain oscillator strength. In the stressed material the dipole operator transforms like Γ_2 and Γ_4 for the directions parallel, (110), and perpendicular, (110), to the external stress axis, respectively. Therefore, according to the resulting selection rules two Γ_2 (Γ_4) excitons

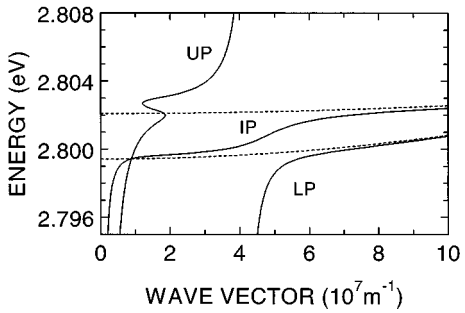

FIG. 1. Dispersion of excitons (dotted lines) and polaritons (solid lines) in a ZnSe epilayer under tensile biaxial strain. LP, IP, and UP denote the lower, intermediate, and upper polariton branch, respectively. $F_1=4.8\times10^{-3}$, $F_2=1.6\times10^{-3}$, $E_1=2.80209$ eV, $E_2=2.79942$ eV, $\Gamma_1=0.2$ meV, $\Gamma_2=0.4$ meV, $\epsilon_b=8.7$, $M_{\rm lh}=0.27m_0$, $M_{\rm hh}=0.81m_0$.

should be observed if the electric vector of the incident light is polarized parallel (perpendicular) to the external stress axis.

B. Line-shape analysis

It is necessary to consider the exciton-photon coupling to obtain the exact positions of the exciton resonances from a reflectance spectrum.[17] First, we use a two-oscillator model to describe the polariton.[18] Therefore, the dielectric function reads

$$\varepsilon(Q,E)=\frac{\hbar^2c^2Q^2}{E^2}=\varepsilon_b+\sum_{i=1}^{2}\frac{X_i}{\varepsilon+Y_i}, \tag{3}$$

$$X_i=\frac{E_{{\rm ex},i}F_i}{E^2}M_ic^2, \quad Y_i=\frac{E_{{\rm ex},i}^2-E^2-iE\Gamma_i}{E_{{\rm ex},i}E^2}M_ic^2, \tag{4}$$

where Q is the wave vector, ε_b is the background dielectric constant, $E_{{\rm ex},i}$ are the energies, M_i are the masses, F_i are the oscillator strengths, and Γ_i are the damping constants of the excitons. The dispersion relation of the three resulting polaritons is shown in Fig. 1.

For small values of the wave vector Q the lower polariton branch (LP) is photonlike while the upper branch (UP) is hh-exciton-like. For increasing Q values the opposite situation is obtained, the LP gets lh exciton character, and the UP shows photonic behavior. A third intermediate polariton branch (IP) changes its behavior from lh exciton to hh exciton character. As an effect of damping all dispersion curves extend down to the origin, whereas for $\Gamma=0$ only the lower branch reaches the origin. The existence of two additional branches in the spectral regime below the energy position of the lowest exciton resonance is not so meaningful because their respective wave vectors are small compared with the photonlike LP. The irregular loop in the UP near the energy of the hh exciton is also caused by damping.

In the second step, we have to calculate the wave propagation. This is done by using a simple dead-layer model. The incident light, described by the electric field amplitude E_i, passes through an exciton-free dead layer with n_b as a frequency-independent refractive index. In the crystal the photon is coupled with two excitons and forms three polaritons. There is no need to consider the back reflection of polaritons at the end of the crystal because all samples are thicker than 2 μm. By taking into account the Maxwell boundary conditions at all boundaries and the additional boundary conditions of Pekar[19] at the dead-layer–crystal interface we are able to determine the reflectivity R:

$$R=\left|\frac{E_r}{E_i}\right|^2=f(E_{\rm ex}). \tag{5}$$

E_r denotes the electric field amplitude of the reflected light.

C. Strain Hamiltonian

A fit of R to the measured reflectivity yields the transverse exciton energies. For a theoretical analysis of the pressure dependence of these exciton states, we follow the theory of Cho.[12] The eightfold subspace of the $1S$ exciton is spanned by the Γ_8 valence band (fourfold) and the Γ_6 conduction band (twofold) of the unstrained material. For this space we have to consider the effects of strain, electron-hole exchange interaction, and the influence of a finite center-of-mass wave vector. The total Hamiltonian reads

$$H=H_{\rm disp}+H_{\rm strain}+H_{\rm exch}. \tag{6}$$

The dispersive term $H_{\rm disp}$ contains the excitonic center-of-mass wave vector Q

$$H_{\rm disp}=\frac{\hbar^2}{2m_0}\Big\{A_1Q^2-A_2\Big[\Big(J_x^2-\frac{1}{3}J^2\Big)Q_x^2+{\rm c.p.}\Big] -A_3(2\{J_x,J_y\}Q_xQ_y+{\rm c.p.})\Big\}, \tag{7}$$

with

$$A_1=\frac{m_0}{M_{\rm ex}}, \quad A_2=-\frac{2\gamma_2m_0^2}{(\gamma_1M_{\rm ex})^2}, \quad A_3=-\frac{2\gamma_3m_0^2}{(\gamma_1M_{\rm ex})^2},$$

$$M_{\rm ex}=m_{\rm el}^*+\frac{m_0}{\gamma_1} \tag{8}$$

J is the hole quasi-spin operator for the Γ_8 valence band, m_0 the electron mass, $m_{\rm el}^*$ the Γ_6 conduction-band electron mass, and the A_i are combinations of the Luttinger parameters γ_i. $H_{\rm strain}$ describes external and internal strain effects[20]

$$H_{\rm strain}=-a\,{\rm tr}(\epsilon)-b[(J_x^2-\tfrac{1}{3}J^2)\epsilon_{xx}+{\rm c.p.}] -(2/\sqrt{3})d(\{J_x,J_y\}\epsilon_{xy}+{\rm c.p.}). \tag{9}$$

a, b, and d are the hydrostatic deformation potential, the tetragonal deformation potential along (100), and the trigonal deformation potential along (111), respectively. The tensor components ϵ_{ij} of the elongation tensor are calculated from the stress components σ_{ij} and the pressure- and temperature-dependent elastic constants c_{ij} that were measured by Lee.[21]

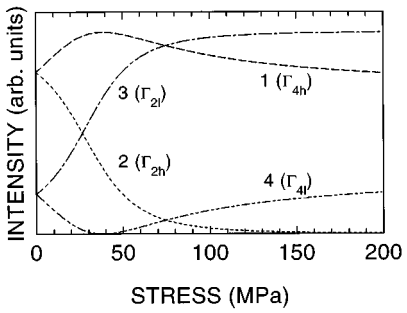

FIG. 2. Evaluated oscillator strengths of the 1S excitons for a tensily strained ZnSe/GaAs heterostructure.

The exchange term H_{exch} includes the analytic and the nonanalytic parts of the exchange interaction between electron and hole (H_{LT} describes the longitudinal-transverse splitting)

$$H_{\mathrm{exch}}=\Delta_0+\Delta_1\vec{\sigma}\cdot\vec{J}+H_{\mathrm{LT}}. \tag{10}$$

Δ_i denotes the exchange parameters, and σ is the electron quasi-spin operator.

The anisotropic exchange effects as well as linear terms in Q are neglected. Taking into account the eight exciton wave functions given by Eq. (2) we are able to diagonalize the whole Hamiltonian. For $Q\|(001)$, we obtain an $(8\otimes 8)$ matrix [Eq. (11)] that separates into three smaller blocks:

	$\|2,+\rangle$ $\|2,-\rangle$	$\|2,0\rangle$ $\|z\rangle$	$\|1,+\rangle$ $\|1,-\rangle$ $\|x\rangle$ $\|y\rangle$
$\|2,+\rangle$ $\|2,-\rangle$	H_1	0	0
$\|2,0\rangle$ $\|z\rangle$	0	H_2	0
$\|1,+\rangle$ $\|1,-\rangle$ $\|x\rangle$ $\|y\rangle$	0	0	H_3

(11)

with

$$H_1=\begin{pmatrix} E(\Gamma_3)+S+2V-\tilde{a}+\tilde{b} & i\tilde{d} \\ -i\tilde{d} & E(\Gamma_4)+S+2V-\tilde{a}-\tilde{b}\end{pmatrix}, \tag{12}$$

$$H_2=\begin{pmatrix} E(\Gamma_3)+S-2V-\tilde{a}-\tilde{b} & i\tilde{d} \\ -i\tilde{d} & E(\Gamma_5^L)+S-2V-\tilde{a}+\tilde{b}\end{pmatrix}, \tag{13}$$

$$H_3=\begin{pmatrix} E(\Gamma_4)+S-V \\ -\tilde{a}+\tilde{b}/2 & (\sqrt{3}/2)\tilde{d} & -\sqrt{3}V+(\sqrt{3}/2)\tilde{b} & \frac{1}{2}\tilde{d} \\ (\sqrt{3}/2)\tilde{d} & E(\Gamma_4)+S-V \\ & -\tilde{a}+(\tilde{b}/2) & -\frac{1}{2}\tilde{d} & \sqrt{3}V-(\sqrt{3}/2)\tilde{b} \\ -\sqrt{3}V+(\sqrt{3}/2)\tilde{b} & -\frac{1}{2}\tilde{d} & E(\Gamma_5^T)+S+V \\ & & -\tilde{a}-(\tilde{b}/2) & (\sqrt{3}/2)\tilde{d} \\ \frac{1}{2}\tilde{d} & \sqrt{3}V-(\sqrt{3}/2)\tilde{b} & (\sqrt{3}/2)\tilde{d} & E(\Gamma_5^T)+S+V \\ & & & -\tilde{a}-(\tilde{b}/2)\end{pmatrix}, \tag{14}$$

where

$$S=\frac{\hbar^2Q^2A_1}{2m_0}, \quad V=\frac{\hbar^2Q^2A_2}{2m_0}, \tag{15}$$

$$\tilde{a}=a(2\epsilon_{xx}+\epsilon_{zz}), \quad \tilde{b}=b(\epsilon_{zz}-\epsilon_{xx}), \quad \tilde{d}=d\epsilon_{xy}. \tag{16}$$

Only the Γ_5 states are dipole allowed in T_d. Regarding the experiment we restrict ourselves to the transverse states $|x\rangle$ and $|y\rangle$. Thus, we have to consider the $(4\otimes 4)$ submatrix H_3 that yields a mixing between the Γ_4 paraexcitons ($|1+\rangle$ and $|1-\rangle$) and the Γ_5 orthoexcitons ($|x\rangle$ and $|y\rangle$). The values of the nondiagonal elements of this matrix depend on the strain and on the center-of-mass wave vector, which, hence, are responsible for a transfer of oscillator strength to the paraexcitons. In total, there are four detectable resonances. The results of the numerical diagonalization of H_3 are shown in Figs. 2 and 3. The evaluated energies

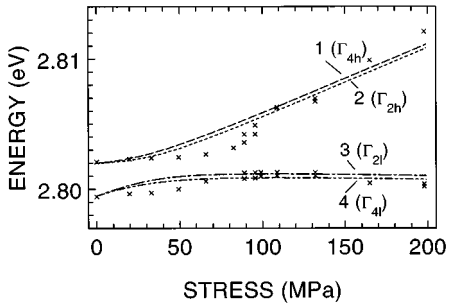

FIG. 3. Exciton peak position vs external stress for a tensily strained ZnSe/GaAs heterostructure. Crosses and lines characterize experiment and theory, respectively.

and oscillator strengths strongly depend on the external stress.

IV. EXPERIMENTAL RESULTS

A. ZnSe/GaAs heterostructures

Figure 4 shows the excitonic reflectance of a 5.3-μm-thick ZnSe/GaAs heterostructure for different external stresses of increasing strength. Polarization-dependent spectroscopy is performed to separate the distinct resonances. The incident light is linearly polarized parallel (π) or perpendicular (σ) with respect to the axis of external stress. The measured four exciton resonances are denoted by the numbers 1 to 4. As predicted in Chap. 3 we observe two resonances for each polarization, i.e., the excitons 2 and 3 in the π polarization, and the resonances 1 and 4 in the σ polarization.

By varying the external stress from 0 to 198 MPa we find a pronounced change in the energy positions and oscillator strengths of the excitons. At 0 MPa the hh-lh splitting is detected, being well known for purely biaxially strained epilayers. The application of uniaxial stress induces the appearance of three excitons as shown in the 33-MPa spectra. The resonances 1 and 3 shift to higher energies, while the exciton

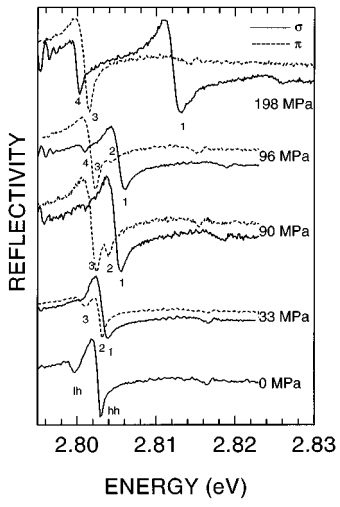

FIG. 4. Reflectance spectra of a 5.3-μm ZnSe epilayer under different external stresses. Solid and dotted lines refer to σ and π polarization, respectively.

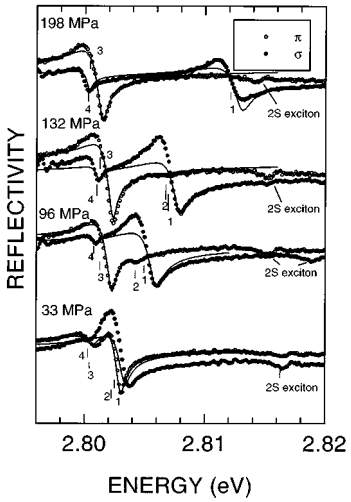

FIG. 5. Line-shape analysis of the measured reflectance. Dots and lines characterize experiment and theory, respectively.

2 hardly changes its position. The fourth resonance is not yet detectable due to its small oscillator strength. If the external stress increases to about 90 MPa, oscillator strength is shifted from resonance 2 to 3, as is visible in the π configuration. The effect becomes more pronounced at higher pressure, where the exciton 2 vanishes gradually. In the σ configuration, the resonance 1 dominates the spectra throughout the whole stress regime. For stresses of 90 MPa and higher an additional resonance 4 is clearly seen. For highest external stress (198 MPa) we observe a dominant splitting into two groups of resonances, where the low-energy group (excitons 3 and 4) represents a polarization-dependent fine structure—similar to the case of pure (110) stress.[20] The large shift and splitting into two groups correspond to expectation concerning the valence and conduction band, and the excitonic fine structure is due to a pressure-induced oscillator strength enhancement of a paraexciton.

The qualitative behavior of the different resonances is in good agreement with the calculated eigenvectors of the Hamiltonian H_3. The observed relative oscillator strengths correspond well to those evaluated from the $|x\rangle$ and $|y\rangle$ contributions to the four new eigenstates, which are shown in Fig. 2.

The pressure dependence of the observed energy positions of the resonances (crosses) is plotted along with the calculated eigenvalues of H_3 (lines) in Fig. 3, in the sense that the lines present a best fit of the solutions of the perturbation theory to the experimental data. We used $a=-5.1\pm0.5$ eV and $d=-3.9\pm0.2$ eV for the deformation potentials, $\epsilon_{xx}=(0.042\pm0.004)\%$ for the internal strain, and $\Delta_1=0.10\pm0.05$ meV for the exchange parameter. The well-known tetragonal deformation potential $b=1.2$ eV (Ref. 22) was chosen as a fixed parameter. The measured stress dependence of the energy positions is well reproduced. Some deviations between 30 and 100 MPa are due to problems in the determination of the different exciton resonances, which are very closely lying in this stress regime.

To confirm the fit results we compared the line shape of the measured reflectance with the line shape calculated after Eq. (5). Figure 5 shows the results for some selected spectra. The lines and dots stand for the theoretical and measured

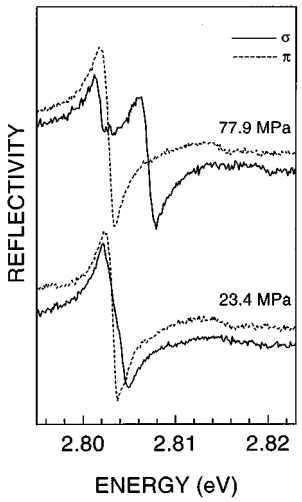

FIG. 6. Reflectance spectra of a ZnSe bulk crystal under external uniaxial stress in (111) direction.

reflectance, respectively. The energies and oscillator strengths that are needed for the calculation are obtained from the diagonalization of H_3 with the parameters mentioned above. Just the damping is varied; it increases slowly with increasing external stress. The contributions of different excitons with their overlapping reflection loops are well reproduced concerning the energy positions and oscillator strengths. The overswinging at the low-energy side of each resonance is caused by the multilayer conception of the lineshape model used. Concerning the energy positions of the excitons some deviations are observed in the 33-MPa spectra. They can be explained by the experimental error in determining the external stress. The deviations at the resonance 1 in the 198-MPa spectrum are caused by a pressure-induced transfer of oscillator strength of the 1S exciton to higher excited states. This would be described by a term in the Hamiltonian that is linear in the angular momentum of the envelope motion. Such a term is not included in our theory.

In conclusion, there is good agreement between both theoretical and experimental reflectance spectra throughout the whole pressure regime.

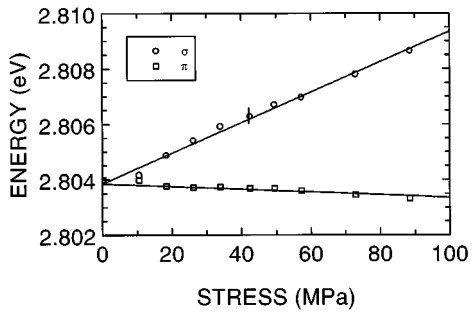

FIG. 7. Stress-induced splitting of the 1S exciton in ZnSe bulk material. Circles and squares characterize the experimental peak positions, the lines show a fit of the eigenvalues of the strain Hamiltonian.

B. ZnSe bulk crystals

Little work has been done so far concerning the determination of the trigonal deformation potential d (Refs. 9 and 11) even for bulk material. To get more information on it, and, thus, to support its value as obtained above in Sec. IV A, we performed reflectance spectroscopy of bulk ZnSe under uniaxial pressure. The stress axis was chosen parallel to the (111) crystal axis to avoid the influence of the tetragonal deformation potential.

The measured reflectance is shown in Fig. 6. No pronounced effect of the exchange interaction is recognizable. Therefore, the excitons are classified by their Γ_8 hole states. In this sense, a line-shape analysis is not necessary, and the energy positions of the excitons are simply taken from the minima of the reflection loops. In Fig. 7 the exciton energies are plotted versus the external stress. A linear splitting pattern into two branches is found. The circles are obtained from the high-energy loop in the σ polarization, and the squares are taken from the low-energy resonance in the π polarization. The observed behavior is caused by the well-known hh-lh splitting of the valence band. It can be explained by a simple diagonalization of H_{strain}.[20] The lines in Fig. 7 are obtained from a fit of the eigenvalues of H_{strain} to the experimental data. This procedure yields $a=-4.9\pm0.5$ eV and $d=-4.3\pm0.2$ eV for the deformation potentials.

TABLE I. Deformation potentials of ZnSe (''–'' sign omitted).

a (eV)	d (eV)	Method	Reference
5.4	3.8	Reflectance under uniaxial stress	9 (after 22)
5.4		Photoluminescence of biaxially strained ZnSe/GaAs	26
5.26		Reflectance of biaxially strained ZnSe/GaAs	25
5.1		Photoluminescence under uniaxial stress	28
4.9		One-photon absorption under hydrostatic pressure	7
4.87		Photoluminescence of biaxially strained ZnSe/GaAs	24
4.8		One-photon absorption under hydrostatic pressure	6
4.65	4.25	Two-photon absorption under uniaxial stress	11
4.5		Two-photon absorption under hydrostatic pressure	8
4.37		Photoluminescence under hydrostatic pressure	27
5.71		Tight-binding calculations	29
5.1	3.9	Reflectance of externally stressed ZnSe/GaAs	This work
4.9	4.1	Reflectance of externally stressed ZnSe bulk	This work

A comparison to values of deformation potentials as found in the literature is sometimes difficult, because the used elastic moduli are often not given therein. A different choice of these parameters (a variety of parameter values can be obtained from the literature, see Ref. 23) yields deviations up to 5%. Regarding this, our results for the hydrostatic deformation potential are in good agreement with published values, as mentioned in Table I for three different kinds of measurements. At first, there are measurements on biaxially strained heterostructures without any external stress.[24–26] Here, the inaccuracy of measuring is large because only one measuring point is available. A second category is defined by measurements under hydrostatic pressure, where the photoluminescence[27] and absorption measurements[7,8] yield a great variety of data ranging from -4.37 eV up to -4.9 eV for the hydrostatic deformation potential. The last kind of measurement is performed under uniaxial stress. This accurate method allows one to determine both the hydrostatic and the trigonal deformation potential. Concerning the hydrostatic parameter the values vary from -4.65 eV (Ref. 11) over -5.1 eV (Ref. 28) up to -5.4 eV (Ref. 9). To our knowledge there exist only two reports yielding the trigonal deformation potential. The respective results again differ, -3.8 eV (Ref. 9) was obtained from reflectance spectroscopy and -4.25 eV (Ref. 11) from two-photon absorption. The latter value fits well to our present data for bulk material.

With regard to the errors of our fit parameters the results obtained on ZnSe bulk material confirm the deformation potential values determined on epilayers (Sec. IV A).

V. CONCLUSION

We performed reflectance spectroscopy of ZnSe/GaAs heterostructures under uniaxial stress. This system serves as a model system for strained-layer heterostructures. By applying a uniaxial stress along (110) on ZnSe epilayers grown in the (001) direction on GaAs substrates, we obtained the hydrostatic deformation potential $a=-5.1\pm0.5$ eV and the trigonal deformation potential $d=-3.9\pm0.2$ eV. This method offers the fundamental possibility to determine deformation potentials in strained-layer heterostructures. Since only two values for the trigonal deformation parameter are found in the literature, we also performed measurements on bulk ZnSe to obtain more reliable information on this potential. By using reflectance spectroscopy under uniaxial stress parallel to the (111) crystal axis we got $a=-4.9\pm0.5$ eV and $d=-4.3\pm0.2$ eV.

The obtained hydrostatic deformation potentials were in good agreement with the data found in the literature. The values for the trigonal deformation potential represent an ingenious extension of the data available so far.

[1] M.A. Haase, J. Qiu, J.M. De Puydt, and H. Cheng, Appl. Phys. Lett. **59**, 1272 (1991).

[2] G. Landwehr and D. Hommel, Phys. Status Solidi B **187**, 269 (1995).

[3] Y. Zhang, B.J. Skromme, and F.S. Turco-Sandroff, Phys. Rev. B **46**, 3872 (1992).

[4] H. Mayer, U. Rössler, S. Permogorov, H. Stolz, H. Vogelsang, and W. von der Osten, J. Cryst. Growth **138**, 195 (1994).

[5] S. Permogorov, H. Stolz, H. Vogelsang, Th. Weber, W. von der Osten, P. Kuznetov, A.N. Pechonov, and A.S. Nasibov, Solid State Commun. **88**, 705 (1994).

[6] S. Ves, K. Strössner, N.E. Christensen, C.K. Kim, and M. Cardona, Solid State Commun. **56**, 479 (1994).

[7] G.F. Schötz, E. Griebl, H. Stanzl, T. Reisinger, and W. Gebhardt, Mat. Sci. Forum **182-184**, 271 (1995).

[8] A. Mang, K. Reimann, and S. Rübenacke, in *Proceedings of the International Conference on the Physics of Semiconductors, Vancouver, 1994*, edited by D.J. Lockwood (World Scientific, Singapore, 1995), p. 317.

[9] D.W. Langer, R.N. Euwema, K. Era, and T. Koda, Phys. Rev. B **2**, 4005 (1970).

[10] D.D. Sell, S.E. Stokowski, R. Dingle, and J.V. DiLorenzo, Phys. Rev. B **7**, 4568 (1973).

[11] D. Fröhlich, W. Nieswand, U.W. Pohl, and J. Wrzesinski, Phys. Rev. B **52**, 14 652 (1995).

[12] K. Cho, Phys. Rev. B **14**, 4463 (1976).

[13] P. Ruppert, D. Hommel, T. Behr, H. Heinke, and A. Waag, G. Landwehr, J. Cryst. Growth **138**, 48 (1994).

[14] M. Heuken, J. Cryst. Growth **146**, 570 (1995).

[15] I. Balslev, Rev. Sci. Instrum. **38**, 1528 (1967).

[16] G.F. Koster, J.O. Dimmock, R.G. Wheeler, and H. Statz, *Properties of the Thirty-Two Point Groups* (MIT Press, Cambridge, MA, 1963).

[17] J.J. Hopfield, Phys. Rev. **112**, 1555 (1958).

[18] H. Leiderer, G. Jahn, M. Silberbauer, W. Kuhn, H.P. Wagner, W. Limmer, and W. Gebhardt, J. Appl. Phys. **70**, 398 (1991).

[19] S.I. Pekar, Zh. Éksp. Teor. Fiz. **33**, 1022 (1957) [Sov. Phys. JETP **6**, 785 (1958)].

[20] G.L. Bir and G.E. Pikus, *Symmetry and Strain-Induced Effects in Semiconductors* (Wiley, New York, 1974).

[21] B.H. Lee, J. Appl. Phys. **41**, 2984 (1970); **41**, 2988 (1970).

[22] A. Blacha, H. Presting, and M. Cardona, Phys. Status Solidi B **126**, 11 (1984).

[23] *Semiconductors. Physics of II-VI and I-VII Compounds, Semimagnetic Semiconductors*, edited by O. Madelung, Landolt-Börnstein, New Series, Group III, Vol. 17, Pt. b (Springer-Verlag, Heidelberg, 1982).

[24] R.L. Gunshor, L.A. Kolodziejski, M.R. Melloch, M. Vaziri, C. Choe, and N. Otsuka, Appl. Phys. Lett. **50**, 200 (1987).

[25] Y.R. Lee, A.K. Ramdas, L.A. Kolodziejski, and R.L. Gunshor, Phys. Rev. B **38**, 13 143 (1988).

[26] K. Shazad, D.J. Olego, and C.G. van de Walle, Phys. Rev. B **38**, 1417 (1988).

[27] J.A. Tuchman, S. Kim, Z. Sui, and I.P. Herman, Phys. Rev. B **46**, 13 371 (1992).

[28] H.L. Cotal, J.B. Maxson, and S.W.S. McKeever, Appl. Phys. Lett. **64**, 1532 (1994).

[29] D. Bertho, D. Boiron, A. Simon, C. Jouanin, and C. Priester, Phys. Rev. B **44**, 6118 (1991).